Available online at www.sciencedirect.com
SciVerse ScienceDirect
www.elsevier.com/locate/brainres

Research Report

Optogenetic drive of neocortical pyramidal neurons generates fMRI signals that are correlated with spiking activity

I. Kahn[a,b,*,1], U. Knoblich[c,1], M. Desai[c], J. Bernstein[c,d], A.M. Graybiel[c], E.S. Boyden[c,d], R.L. Buckner[a,b,e], C.I. Moore[c,2]

[a]Center for Brain Science, Harvard University, Cambridge, MA, USA
[b]Athinoula A. Martinos Center for Biomedical Imaging, Massachusetts General Hospital, Charlestown, MA, USA
[c]McGovern Institute for Brain Research and Department of Brain and Cognitive Sciences, MIT, Cambridge, MA, USA
[d]The MIT Media Laboratory, Synthetic Neurobiology Group, and Department of Biological Engineering, MIT, Cambridge, MA, USA
[e]Departments of Psychiatry and Radiology, Massachusetts General Hospital, Boston, MA, USA

ARTICLE INFO

Article history:
Accepted 6 March 2013
Available online 21 March 2013

Keywords:
fMRI
Hemodynamic response function
Somatosensory cortex
Barrel cortex
Multi-unit activity
Cell-attached recording
Local field potential

ABSTRACT

Local fluctuations in the blood oxygenation level-dependent (BOLD) signal serve as the basis of functional magnetic resonance imaging (fMRI). Understanding the correlation between distinct aspects of neural activity and the BOLD response is fundamental to the interpretation of this widely used mapping signal. Analysis of this question requires the ability to precisely manipulate the activity of defined neurons. To achieve such control, we combined optogenetic drive of neocortical neurons with high-resolution (9.4 T) rodent fMRI and detailed analysis of neurophysiological data. Light-driven activation of pyramidal neurons resulted in a positive BOLD response at the stimulated site. To help differentiate the neurophysiological correlate(s) of the BOLD response, we employed light trains of the same average frequency, but with periodic and Poisson distributed pulse times. These different types of pulse trains generated dissociable patterns of single-unit, multi-unit and local field potential (LFP) activity, and of BOLD signals. The BOLD activity exhibited the strongest correlation to spiking activity with increasing rates of stimulation, and, to a first approximation, was linear with pulse delivery rate, while LFP activity showed a weaker correlation. These data provide an example of a strong correlation between spike rate and the BOLD response.

This article is part of a Special Issue entitled Optogenetics (7th BRES)

*Corresponding author. Current address: Department of Physiology and Biophysics, Rappaport Faculty of Medicine, Technion—Israel Institute of Technology, Haifa 32000, Israel. Fax: +972 4 829 5461.
E-mail address: kahn@technion.ac.il (I. Kahn).
[1]These authors contributed equally to this report.
[2]Current address: Department of Neuroscience and Brown Institute for Brain Sciences, Brown University, Providence, RI 02912, USA.

0006-8993/$ - see front matter © 2013 Elsevier B.V. All rights reserved.
http://dx.doi.org/10.1016/j.brainres.2013.03.011

1. Introduction

The blood oxygenation level-dependent (BOLD) functional magnetic resonance imaging (fMRI) signal is widely used to study human brain organization. Because this response measures hemodynamic fluctuations, and not the underlying neurophysiological signals that most researchers are mainly interested in, the correlation between neural activity and the BOLD fMRI signal has been studied extensively (Boynton et al., 1996; Dale and Buckner, 1997; Heeger et al., 2000; Logothetis et al., 2001; Miezin et al., 2000; Mukamel et al., 2005; Rees et al., 2000; Shmuel et al., 2006; Viswanathan and Freeman, 2007). Several reports have emphasized the close coupling between local field potential (LFP) activity and BOLD activity (or other measures of the hemodynamic response), de-emphasizing correlations to single-unit and multi-unit action potential (spiking) activity (Logothetis et al., 2001; Sirotin and Das, 2009; Viswanathan and Freeman, 2007).

These reports provide examples of correlations between LFP and BOLD responses when sensory input is used to induce neural activity. However, sensory input drives an ensemble of cell types in the neocortex and connected subcortical regions, and likely recruits neuromodulatory pathways as well (Fournier et al., 2004; Kirifides et al., 2001; Shima et al., 1986), pathways that may not evoke local spikes but are well known to impact local hemodynamics. Even the simplest sensory input will, through feedforward thalamic drive, activate a broad complement of local cell types including pyramidal neurons, fast-spiking interneurons and astrocytes, among others (Schummers et al., 2008; Simons and Carvell, 1989; Swadlow, 1989; Wang et al., 2006). As such, past attempts to understand the neural correlates of the BOLD signal are chiefly observed in the context of a complex barrage of input activity arriving in a neocortical area.

Given the history of such correlation studies, and the current bias to viewing the BOLD signal as best correlated with the LFP, an important unresolved issue is whether, and if so under what conditions, spiking activity might be strongly correlated with the BOLD signal. In support of the possibility that such conditions might exist, Rees et al. (2000) used cross-species correlations to argue that in human area MT+, fMRI responses increase in proportion to the increase in single-neuron spiking in monkey area MT (see Heeger, et al. 2000 for a similar analysis in area V1 of human and monkey; see also Boynton et al., 1996; Dale and Buckner, 1997; Miezin et al., 2000). Similarly, Mukamel et al. (2005) compared activity of individual neurons in the auditory cortex of patients implanted with depth electrodes and fMRI recordings from a separate group of healthy participants, and found that spiking activity was correlated with BOLD responses during presentations of naturalistic stimuli. Thus, in contrast to the widely held interpretation that postsynaptic subthreshold activity, which is a key component of the LFP, is the correlate of the BOLD signal, these additional studies suggest that there are regimes in which spiking activity in the neocortex may be the better correlate of the local BOLD response (for reviews see Heeger and Ress, 2002 and Logothetis, 2008).

To precisely control local neural activity in studying its correlation to the BOLD signal, we employed an 'Opto-fMRI' approach. Similar to recent demonstrations (Desai et al., 2011; Kahn et al., 2011; Lee et al., 2010), we combined activation of the microbial opsin channelrhodopsin-2 (ChR2), a light sensitive nonselective cation channel (Boyden et al., 2005), with high-field functional imaging (9.4 T fMRI). Extracellular recording studies in sensory neocortex of primates—the preparation and cortical area used for most previous studies of BOLD correlates—primarily monitor spike activity of large pyramidal neurons, such as those in layer V. We therefore employed as a model preparation the *Thy1*-ChR2-YFP mouse, as ChR2 is selectively expressed in neocortical pyramidal neurons, primarily those in layer V throughout the neocortex (Arenkiel et al., 2007). Targeting primary somatosensory cortex, we tested whether increased evoked pyramidal cell spike activity would result in proportional increases in the BOLD response. We also manipulated the statistics of these stimulus trains, using periodic vs. Poisson distributed timing that conserved the overall frequency of light stimulation but evoked distinct patterns of neural responses. We reasoned that this manipulation might provide a way to dissociate the neural correlates of the BOLD response, as these optical stimulation regimes induce different patterns of spiking and subthreshold activity, and unlike behavioral stimuli, are associated with precisely controlled activity in a defined cell type.

We found that the BOLD response evoked in this fashion was linear under conditions of increased spike rate. Across stimulus patterns and analyses, the strongest correlation was observed between spiking activity and the BOLD response, with transfer functions generated based on spiking activity providing an accurate estimation of the measured BOLD response. These data provide evidence for a regime, albeit outside natural physiological parameters, of neural activity in the neocortex in which the BOLD signal is predicted best by local spiking activity.

2. Results

2.1. *Optical drive of layer V pyramidal neurons generates a BOLD response*

We first tested whether a BOLD response could be observed in response to optical stimulation in neurons expressing ChR2. Stimuli were presented for 15 s blocks at a frequency of 40 Hz and 8 ms pulse duration, followed by 15 s of no stimulation, and repeated 16 times in each run. Activation was observed in all *Thy1*-ChR2-YFP mice (Fig. 1; 4 animals; $P<0.05$, corrected for multiple comparisons using family-wise error rate method) but not in wild-type mice (ChR2-YFP negative) that received identical stimulation ($n=2$ mice). In all the animals the observed responses were restricted to the area under the fiber optic.

2.2. *The pattern of light-stimulation impacts the amplitude of the BOLD response*

Increasing the frequency of optical stimulation drives an increased number of spikes in neurons expressing ChR2 in the neocortex in vivo (e.g., see Cardin et al., 2009). To test

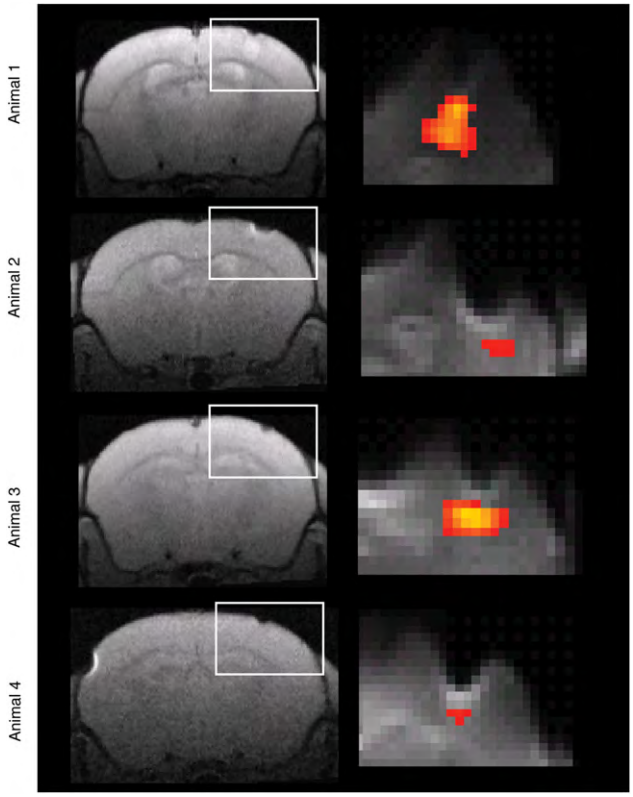

Fig. 1 – Light-evoked pyramidal cell spiking results in a consistent BOLD fMRI response in *Thy*1-ChR2-YFP mice. Activation was observed across all animals. For each individual animal, an anatomical coronal slice where the craniotomy was located and fiber optic inserted is presented (left). The region of stimulation is denoted by a white rectangle. "Localizer" runs consisted of 16 repetitions of 15 s on–15 s off light-pulses at 40 Hz/8 ms pulse duration (4–8 for each animal). A statistical parametric map of a positive BOLD response to light stimulation ($P<0.05$ corrected for multiple comparisons using family-wise error [FWE] correction) is overlaid to demonstrate the extent of response for each animal (right).

whether linearity of the BOLD response would hold across increased frequency of stimulation, we drove pyramidal cells at rates ranging from 8 to 80 Hz for intervals of 15 s with either Poisson or periodic stimulus trains. We sought to compare the BOLD response to the electrophysiological responses. Electrophysiological responses measured were single-unit activity (SUA) with glass pipettes in cell-attached mode, as well as multi-unit activity (MUA) and local field potentials (LFP) with a laminar electrode.

Most animal physiology and human electroencephalography studies record field potentials in alternating current (AC) coupled mode, as was the case for the laminar data collected here. This mode prevents observation of global shifts in signal (the data is by definition high-pass filtered, commonly with a cutoff between 0.1 Hz and 1 Hz). The simultaneous optical drive of a large population of ChR2-expressing neurons applied in this study resulted in highly synchronous currents, and at higher stimulation frequencies the kinetics of ChR2 (Boyden et al., 2005; Ishizuka et al., 2006; Nagel et al., 2003) and the cells' membrane time constant would result in a significant DC component in the subthreshold response (Fig. 2). Therefore, we hypothesized that the amplitude of LFP recorded in direct current (DC) coupled mode (denoted dcLFP) would better reflect the absolute level of electrical current resulting from light-stimulation than the power of LFP recorded in AC coupled mode. This prediction is consistent with an hypothesis linking slow spontaneous fluctuations in the BOLD signal with slow cortical potentials (He and Raichle, 2009) and prior proposals that sensory-driven cortical activity is likely coupled with a change in steady potentials (Goldring, 1974; He and Raichle, 2009). Critically, conventional LFP may not detect this slow response.

To illustrate this point we compared electrophysiological recordings made using the laminar probes (MUA and LFP in alternating current coupled mode [LFP]) and saline-filled glass pipettes (LFP recorded in direct-current mode [dcLFP]) during optical stimulation. Fig. 2 depicts a comparison of responses to 8 and 40 Hz periodic stimulus trains. All measures demonstrated elevated responses for optical drive at both 8 and 40 Hz relative to the pre-trial baseline. Fig. 2A depicts a response for two trials (8 and 40 Hz) measured concurrently with laminar electrode and glass pipette. As can be seen, MUA is higher for 40 relative to 8 Hz but LFP power is higher for 8 relative to 40 Hz. As can be seen for dcLFP, while the amplitude of the oscillatory component is similar to that of the LFP, the overall shift in the signal is higher for 40 relative to 8 Hz. Quantifying this result (Fig. 2B), firing rate (MUA) was elevated ($n=2$ animals) for 40 Hz compared to 8 Hz (Wilcoxon rank-sum test, $P=5.78e-12$), the LFP power ratio ($n=3$) decreased with increased stimulation frequency ($P=0.0134$) and the dcLFP ($n=3$) average voltage amplitude increased from 8 to 40 Hz ($P=3.08e-08$). Finally, we confirmed this interpretation by recording the membrane potential of an individual neuron recorded intracellularly in current clamp mode (Fig. 2C). Thus, dcLFP provides a better measure of currents induced by optical drive, although it is noted that these steady state changes should typically be present in other types of stimulation (e.g., sensory drive).

2.3. *Fidelity of local field potential measurements*

LFP measured from the laminar electrodes demonstrated a steady decline in power in response to an increase in optical stimulation frequency. To discount the possibility that this observation is a result of low pass filtering by the recording amplifier, we quantified the degree of low-pass filtering in our electrophysiological recording setup. We generated sine waves at 1, 2, 5, 10, 20, 50, 100, 200, 500, and 1000 Hz for 20 trials each and computed the power with the spectrogram function, similar to the analysis conducted in our data. In Fig. 3A we plot the results of this computation. The derived transfer function exhibits a 0.7% drop in signal strength from 8 to 80 Hz. Since the change in LFP signal was two orders of magnitude stronger (82%), it is unlikely that this drop can be accounted for by biases (low-pass filtering) in the amplifier setup.

In the analyses described below, the dcLFP amplitude provided a consistently closer estimate for the BOLD response. The dcLFP measurements were carried out with a saline-filled glass pipette that was placed at different

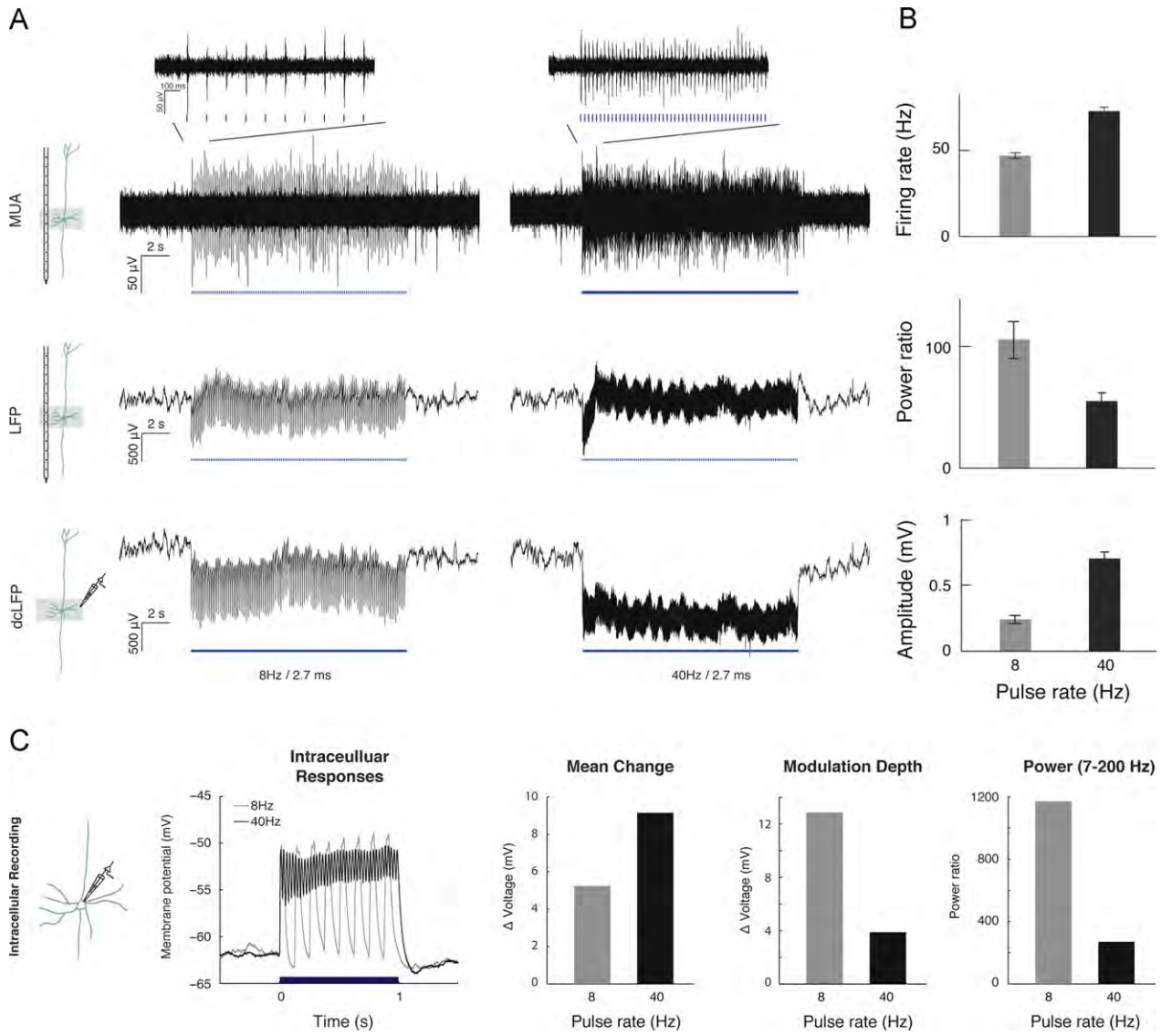

Fig. 2 – High-pass filtered local field potentials (LFP) do not correlate with layer V pyramidal neurons spike activity. LFP acquired in in vivo neurophysiological experiments is traditionally recorded in alternating current coupled mode (effectively filtering frequencies below 0.1–1 Hz; e.g., see ref. Cardin et al., 2009). Consequently, voltage changes that take place on a timescale of seconds are abolished. We compared electrophysiological recordings using laminar probes (MUA and LFP in AC coupled mode [LFP]) and saline-filled glass pipettes (LFP in direct-current mode [dcLFP]) during optical stimulation (8 and 40 Hz at 2.7 ms pulse width). (A) MUA (band-pass filtered between 600 and 6000 Hz), as well as LFP and dcLFP (raw unfiltered signals) are depicted for a representative trial. (B) Firing rate (MUA) is elevated ($n=2$ animals) for 40 Hz compared to 8 Hz, while LFP power ratio ($n=3$ animals) decreased. Consistent with firing rate, dcLFP ($n=3$ animals) average voltage amplitude increased when light stimulation frequency increased. (C) Intracellular in vivo recordings in current clamp mode were carried out to measure the effects of frequency modulation on membrane potential, motivating recording LFP in direct current mode (dcLFP), and explaining power reductions observed with conventional LFP recordings. Here we plot the responses in a cell that showed light-driven subthreshold responses (as determined by latency) but no spiking. Average raw time series (unfiltered) for each condition (8 and 40 Hz with 2.7 ms pulse width) demonstrate the robust effect of 1 s train of light pulses on membrane potential. Notably, an overall shift in membrane potential is observed for 40 but not 8 Hz stimulation. Peak depolarization is equivalent between the two conditions but amplitude of oscillations differs. A quantification of this representative single trial is provided for mean membrane potential change (left), membrane potential modulation depth (middle) and power ratio (right). Mean membrane potential change was higher for 40 relative to 8 Hz, while modulation depth and power ratio, both reflecting the magnitude of oscillation, were higher for 8 relative to 40 Hz trains of light pulses.

depths under the optical stimulation site while the laminar electrode (LFP) was placed once. Consequently, it is possible that the population that is measured by each electrode differs. To discount that possibility, we computed LFP power measured from the glass pipettes. As can be seen in Fig. 3B, LFP power is identical in the two modes of recording,

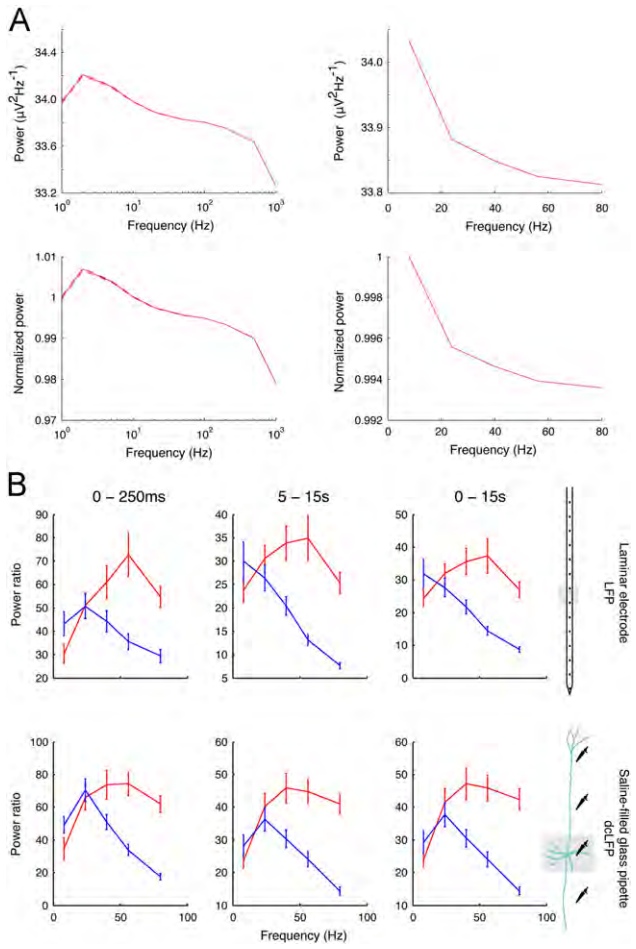

Fig. 3 – Fidelity of local field potential measurements. (A) A sine-wave at multiple frequencies (1, 2, 5, 10, 20, 50, 100, 200, 500, and 1000 Hz) was generated and passed into the amplifier through the headstage (left). The power of the recorded signal was computed and then interpolated at 8, 24, 40, 56, and 80 Hz (right). Comparison of 8 to 80 Hz of normalized power demonstrates that 0.7% reduction is observed. (B) The early, late and entire interval of optical stimulation is compared between the two principal methods for recording LFPs. As depicted, when power of the oscillatory neural activity recorded in direct current coupled mode LFP (dcLFP) is analyzed equivalently to the LFP recorded with the laminar electrodes (recorded in alternating current coupled mode), the resultant graphs show similar responses.

suggesting that the decrement observed in the periodic condition and the broadband response peaking at 40 Hz, indeed reflect neural activity measured with LFP, rather than an artifact of recording method or proximity of the recording electrode to optically-induced pyramidal cell spiking.

2.4. *The BOLD response is best correlated with spiking activity*

We sought to test which of these commonly recorded neural measures provided the best predictor of the BOLD response by manipulating the rate and statistics of optical pulses applied. We chose a comparison of Poisson and periodic regimes to span the range of spiking statistics that might be generated by commonly used sensory stimuli (e.g., sinusoidal visual gratings), naturalistic sensory stimuli, or ongoing internal neocortical dynamics. To determine the neural correlates of these stimulation patterns, we recorded SUA activity in layer V, and LFP, MUA, and dcLFP throughout the neocortical depth, providing a variety of measures (e.g., somatic spiking versus dendritic LFP activity) to compare with the BOLD signal.

The BOLD signal showed a gradual increase in amplitude with increasing rate of stimulation for both periodic and Poisson stimulation, with a greater increase in overall amplitude for Poisson stimuli at all frequencies (Fig. 4A), confirmed as statistically significant by a reliable main effect of stimulation frequency in a two-way ANOVA of Frequency × Regime ($F_{BOLD}(4790)=7.64$, $P<0.001$) and a main effect of stimulation regime ($F_{BOLD}(1790)=6.56$, $P=0.01$). The SUA responses demonstrated a pattern similar to the BOLD response, showing a gradual increase in firing rate and exhibiting an overall higher firing rate for Poisson relative to periodic stimulation (Fig. 4B; main effect of stimulation frequency $F_{SUA}(41,290)=4.12$, $P<0.001$, and regime $F_{SUA}(11,290)=75.22$, $P<0.001$). Responses across the different contacts of the laminar electrode (Fig. 4C,D) revealed that MUA responses driven by light were localized to 700–800 μm depth, reflecting spiking activity in or near layer V, while dendritic and somatic responses were reflected in LFP and dcLFP increases at 100–800 μm depth. Similar to the BOLD and SUA responses, the MUA (Fig. 4D) and dcLFP (Fig. 4E) responses exhibited a monotonic increase in signal as a function of frequency (main effect of Frequency: $F_{MUA}(4390)=52.85$, $P<0.001$, $F_{dcLFP}(4290)=71.55$, $P<0.001$). Similar to BOLD and SUA responses, MUA trended to an overall greater response to Poisson relative to periodic stimulation (main effect of stimulation regime: $F_{MUA}(1390)=3.53$, $P=0.06$). In contrast, unlike BOLD and SUA responses, dcLFP responses did not differ between Poisson and periodic stimulation regimes ($F_{dcLFP}(1290)=0.04$, $P=0.83$). The LFP responses (Fig. 4D) exhibited an overall increase in power for Poisson relative to periodic regimes ($F_{LFP}(1890)=56.97$, $P<0.001$), but did not exhibit a monotonic increase in power with increasing frequency for Poisson stimulation, and showed a monotonic decrease in power for periodic stimulation (expressed by a main effect of Frequency $F_{LFP}(4890)=8.47$, $P<0.001$ and Regime × Frequency interaction $F_{LFP}(4890)=12.62$, $P<0.001$). This pattern was consistent across the different layers for LFP and dcLFP but restricted to layer V for MUA (Fig. 4C–E), confirming that dendritic currents may underlie these responses in LFP and dcLFP.

In sum, spiking activity recorded from optically driven layer V neurons demonstrated the closest similarity to the BOLD response, showing both a monotonic increase in magnitude of responses as a function of frequency, and greater responses for Poisson relative to periodic stimulation. In contrast, LFP showed an inverted U shaped or decreasing function for Poisson or periodic stimulation, respectively.

2.5. *The BOLD response can be derived from spiking activity*

We further examined the relation between neural activity and the BOLD response with two independent approaches.

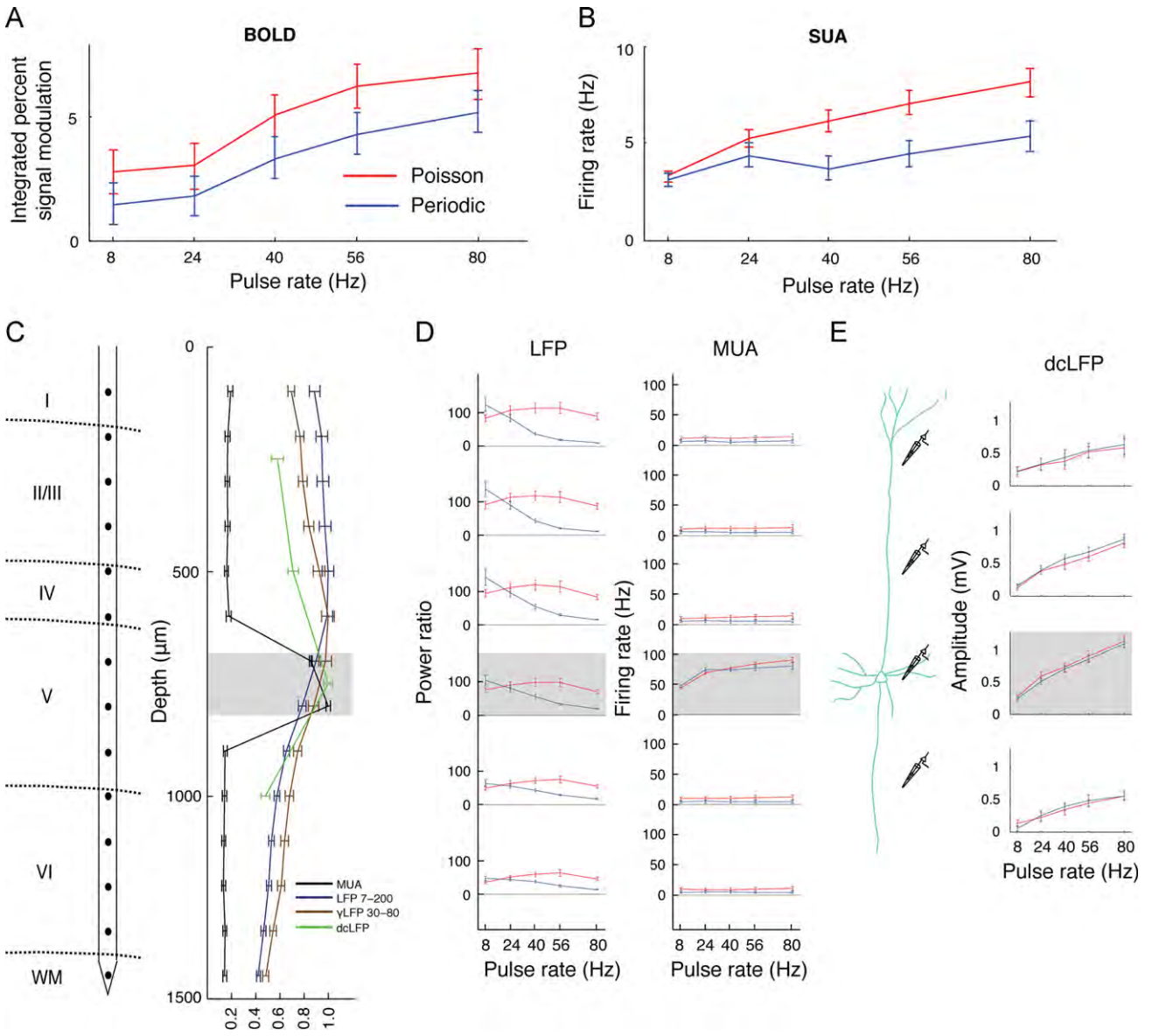

Fig. 4 – Pyramidal neuron spiking and BOLD responses are greater for Poisson relative to periodic optical stimulation. (A) For each animal in the fMRI experiment ($n=4$), time series were extracted from a region of interest (ROI) identified in an independent localizer scan. The integrated BOLD response across the entire stimulation interval (2.5–17.5 s), as determined from the localizer scan, was computed. A monotonic increase in the BOLD signal as a function of stimulation rate and a greater signal increase for Poisson relative to periodic stimulation were observed. (B) Cell-attached single-unit activity (SUA) recordings demonstrated a monotonically increasing spiking rate for both stimulation regimes, and a greater signal increase was observed for Poisson than periodic stimuli. (C) Responses across neocortical layers were measured using 16-contact laminar electrodes with contacts spaced at 100 μm. The normalized responses for LFP power, MUA firing rate and direct current LFP (dcLFP) amplitude are plotted as a function of depth (100–1400 μm). During optical drive, MUA demonstrated a peak response at 700–800 μm with only baseline response elsewhere. In contrast, LFP demonstrated a response that was sustained from 100 μm to 700–800 μm, and dcLFP demonstrated a response that was elevated throughout and peaked at 700–800 μm. (D) Poisson (red) and periodic (blue) regimes drove different LFP responses, yielding a decreased response when the rate of stimulation increased for periodic, and a constant response with a peak at 40–56 Hz for Poisson stimulation. The MUA did not differ between Poisson and periodic stimulation and demonstrated a monotonic increase at 700–800 μm depth for both regimes. (E) The dcLFP demonstrated an increased rate of stimulation for both stimulation regimes with an increased amplitude towards 700–800 μm that was followed by a slight drop at depth 1000 μm.

First, we computed the correlation between neural responses and the BOLD response using polynomial fits of their frequency-dependent modulation. Second, we tested whether the BOLD response could be derived by convolution of the neural signal with a standard hemodynamic response function (HRF).

To test whether the temporal evolution of the BOLD response could be derived from the neural data, we down-sampled our neural measures (SUA and MUA firing rate, LFP power, and dcLFP amplitude) to match the temporal resolution of the BOLD signal (2.5 s), and convolved these metrics with a canonical HRF to yield a predicted BOLD signal time series. The amplitude of the response was determined by least squares estimation of a multiplicative factor. The best predictor of the BOLD signal across stimulation patterns was obtained by measures reflecting spiking activity (SUA and MUA; Fig. 5), mostly due to the lack of an early peak response in the LFP-derived measures. Overall correlation values were higher for Poisson relative to periodic stimulation, with LFP and dcLFP demonstrating the greatest decrease in goodness-of-fit. We tested whether the numerical difference in goodness-of-fit in spiking activity relative to LFP was reliable by a Wilcoxon rank-sum test between MUA ($n=40$ trials) and LFP ($n=90$ trials). In the Poisson condition, MUA did not reliably differ from the LFP signal ($P_{Poisson}=0.85$). However, in the periodic condition, MUA was reliably greater than LFP ($P_{Periodic}=1.11e\text{-}09$). A paired-sample Wilcoxon two-tail signed rank test including only trials where MUA and LFP signals were concurrently available ($n=40$) confirmed that MUA was a better predictor on a trial-by-trial basis for the periodic but not for the Poisson condition ($P_{Poisson}=0.29$; $P_{Periodic}=2.63e\text{-}07$). Taken together, these approaches for deriving the BOLD response from the neural data indicate that under conditions of optical stimulation of ChR2-expressing pyramidal neurons, spiking activity is a more reliable correlate for the BOLD response than the LFP signal.

2.6. *The BOLD response reflects the adaptation dynamics of single unit activity*

Rapid adaptation of neural responses has been reported for pyramidal neurons directly driven with current or with paired synaptic input (Connors and Gutnick, 1990) and during sensory stimulation (Wark et al., 2007). Thalamo-cortical and intracortical synaptic depression, intrinsic firing-rate adaptation and frequency-dependent synaptic inhibition are possible mechanisms (Moore et al., 1999; Moore, 2004). Under the current approach, adaptation of ChR2 itself could also contribute to this decline (Nagel et al., 2003). We posited that one of many possible sources of divergence between our results and prior reports emphasizing a high correlation between BOLD signal and LFP could have arisen from a different interpretation/modeling of these temporal dynamics (Logothetis et al., 2001; Viswanathan and Freeman, 2007).

Utilizing this temporally non-linear relationship between neural input (as measured by LFP) and output (as measured by spiking), we divided the neural response into an early period capturing the initial peak and a late period characterizing the late sustained response (Fig. 6).When comparing the early peak and sustained late periods in the BOLD response and physiological measures, both responses were characterized by an initial strong onset followed by an attenuated but persistent response; however the strength of the adaptation (the ratio between peak and sustained response) differed between the measures.

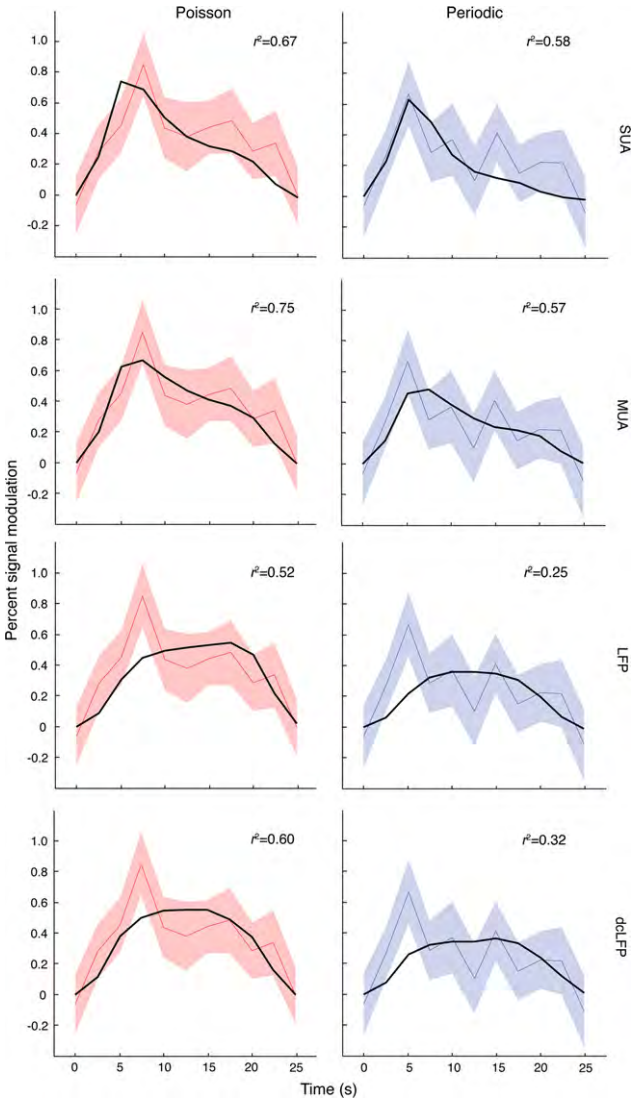

Fig. 5 – BOLD signal time series can be derived from spiking activity. The time series of each measure (SUA and MUA firing rate, LFP power, and dcLFP amplitude) was down sampled to 2.5 s to match the resolution of the BOLD signal and was convolved with a canonical hemodynamic response function, yielding a predicted BOLD signal time series. Predicted time series were computed separately for Poisson and periodic regimes and are plotted here for 40 Hz stimulation rate. The response amplitude was determined by computing a least squares fit (black line) to the measured BOLD signal (Poisson—red line, shade [mean ± sem]; Periodic—blue).

We observed that the magnitude of the initial peak was numerically higher for periodic than Poisson stimulation but the later sustained response was reversed. In contrast, LFP activity exhibited a pattern that diverged from BOLD signal and SUA, a numerically higher response for Poisson than periodic for the whole response interval (Fig. 7A). This observation motivated us to test whether the temporal dynamics of the response were better correlated between spiking and BOLD signal under these conditions. The responses for each of the stimulation frequencies and the Poisson and periodic regimes are shown in Fig. 7A.

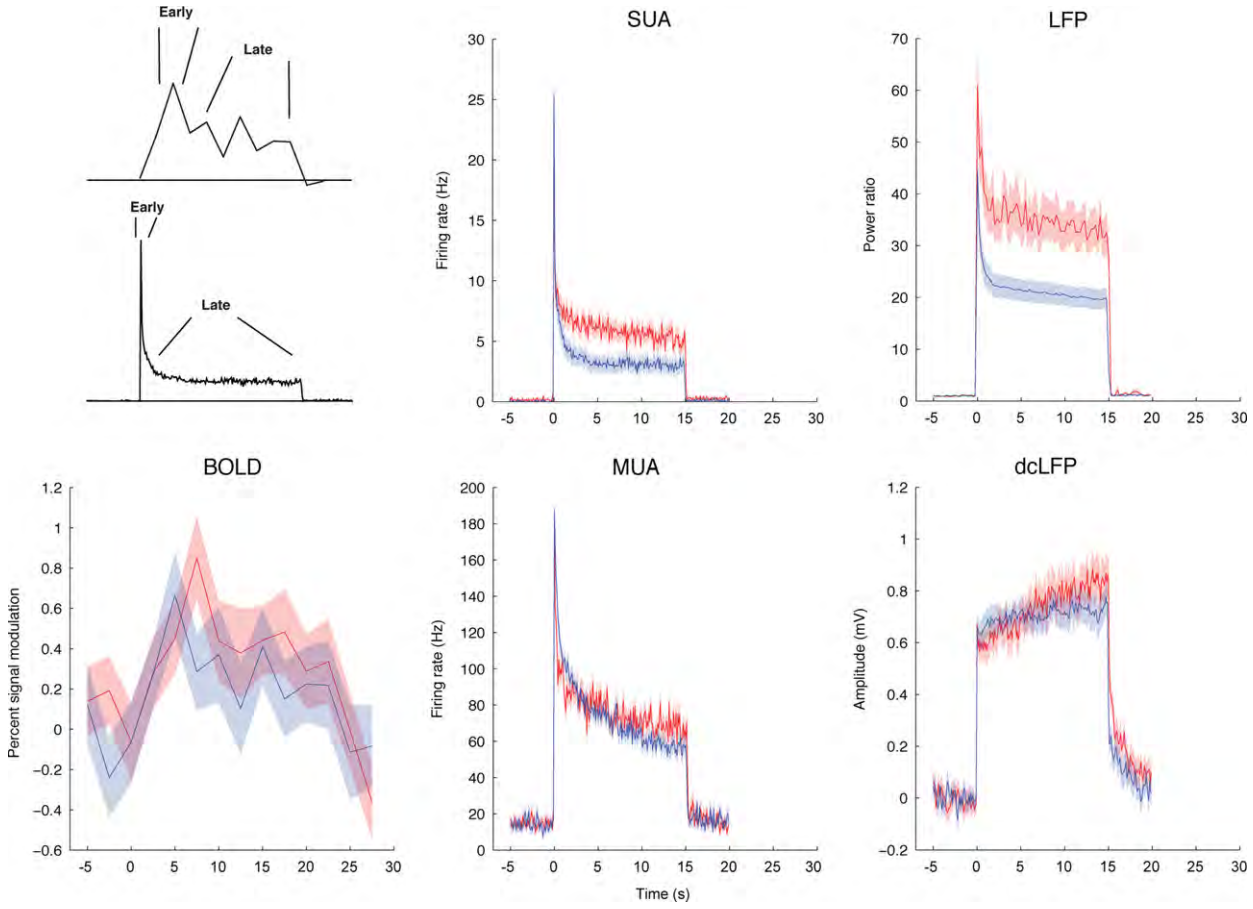

Fig. 6 – Time series for Poisson (red) and periodic (blue) stimulation regimes at 40 Hz. Responses are depicted for BOLD percent signal modulation, SUA and MUA firing rate, LFP power, and dcLFP amplitude. Differences in the amplitude of response between early and late periods as a function of stimulation regimes motivated quantification of this modulation across the different measures.

To quantify this effect, we fitted transfer functions that incorporated the integrated responses to each of the stimulation regimes and frequencies, measuring the extent to which each neural measure predicted the BOLD response. We fitted first or second order polynomial functions, taking into account the responses to both Poisson and periodic regimes and the different rates of light stimulation separately for the early and late periods (Fig. 7B). The SUA, MUA and dcLFP measures yielded better transfer functions than LFP, and LFP restricted to the gamma band when separating to early and late intervals, similar to the transfer functions computed for the whole duration of stimulation (not shown). The second order polynomial yielded similar or better goodness-of-fit values.

One potential caveat in attempting to produce a transfer function between electrophysiological recordings and BOLD signal is the slow timescale of the latter's response. In particular, as demonstrated previously (Goense and Logothetis, 2008), these correlations are strongly dependent on the time scale at which the signals are compared and correlation of SUA, MUA and LFP with the BOLD signal are reduced when considered on slow time scales. While the analysis that derived the BOLD response by convolving it with a canonical HRF (Fig. 5) is impacted by this issue, producing a transfer function for the integrated response across the different stimulation frequencies and pulse train statistics alleviates it. In taking into account the entire response period, and further, by separating into early and late components (the former is likely impacted most by this issue), the present results argue that the better correlation observed for spiking relative to LFP is not a result of differences in timescales.

3. Discussion

Our findings demonstrate that regular spiking pyramidal cells in layer V of the sensory neocortex can be driven by stimulation of light-activated cation channels, producing a hemodynamic response that is reliable and consistent across experimental runs and animals. We observed proportional increases in action potential and LFP signals that were reflected in the BOLD response. We recorded single-unit, multi-unit and LFP activity, and we observed that the BOLD response was best correlated to single-unit and multi-unit activity localized to layer V of the neocortex. The BOLD signal tracked the temporal evolution of spiking activity, reflecting differential modulation of neural activity in individual cells.

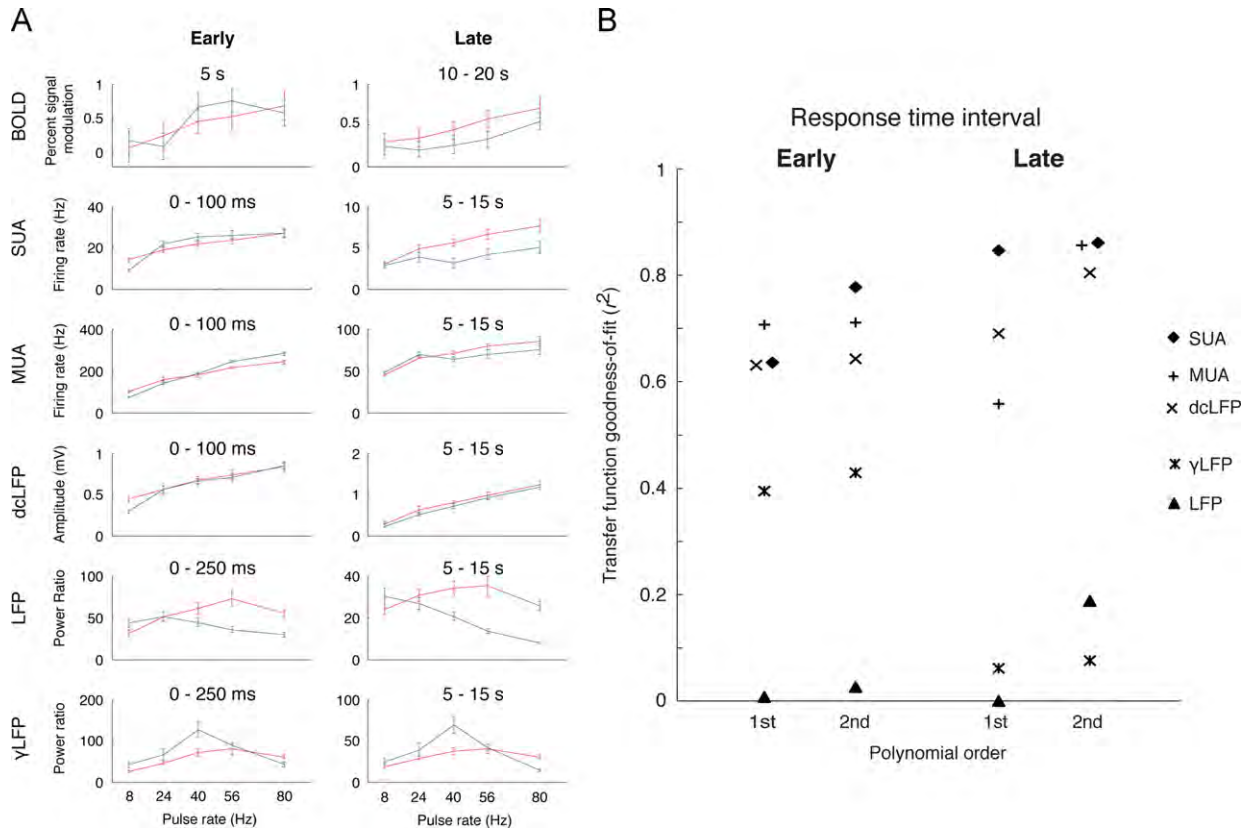

Fig. 7 – Analysis of early and late response components reveal similarity between the BOLD signal and spiking but not LFP measures. (A) Motivated by the differential dynamics observed in the time series of the BOLD signal and electrophysiological measures, we plot here early and late responses as a function of stimulation regime (Poisson and periodic) and frequency. Responses are depicted for BOLD percent signal modulation, SUA and MUA firing rate, dcLFP amplitude, and LFP, and gamma-bandpassed LFP (γLFP) power. (B) Neural to BOLD signal transfer functions were computed by fitting a 1st or 2nd order polynomial to each neural measure (SUA, MUA, LFP, dcLFP, and γLFP). A goodness-of-fit (r^2) is plotted for 1st and 2nd order functions and the early and late response periods.

We used light stimulation to provide precisely timed inputs to cortical neurons to test whether the BOLD response would reflect the evoked neural activity. Our findings provide a quantitative demonstration that the BOLD signal, under these conditions of predominant layer V pyramidal neurons drive, tracks action potential better than postsynaptic subthreshold activity (as reflected by LFP and dcLFP). Optical drive was achieved by inducing light at the surface of the brain, with the light decaying exponentially with cortical depth. Thus, the maximal locus of light could be a generator for both the LFP signal and the action potentials observed. However, MUA activity recorded throughout the layers was maximal and limited to layer V—we did not detect evidence of differential spiking in layers II/III. Further, LFP responses were consistent across layers I–V—effects that would not have occurred were they proportional to light intensity in a simple way (Fig. 4C,D). Instead, the signal measured here appears to be a reflection of dendritic current flow and consequent spiking in layer V neurons (in agreement with a common interpretation of the LFP).

Under the conditions of synchronous high frequency drive of a large population of neurons lasting several seconds utilized in this study, the power in the oscillatory component of the LFP provided a poor measure of the total evoked subthreshold activity. Due to the kinetics of ChR2 (Boyden et al., 2005; Ishizuka et al., 2006; Nagel et al., 2003) and cell membrane, the oscillatory component of the subthreshold response decreased with increased stimulus frequency while the constant component increased (see Fig. 2C). In contrast to the commonly used LFP power, which only evaluates the oscillatory component of the LFP, dcLFP amplitude captures the entire signal including both AC and DC components (note that it is not feasible to measure the amplitude of an AC coupled LFP signal since the DC component has been abolished or at least altered by the high-pass filter). While this study cannot indicate whether the distinction between the two LFP measures is as prominent in natural sensory-driven responses, the data here suggest that such conditions can exist in the neocortex (see also Goldring, 1974). Further, the dcLFP amplitude accurately tracked the increased drive with increased stimulation frequency, but failed to distinguish between periodic and Poisson timing. One possible explanation is that secondary sub- and supra-threshold activity not directly induced by optical drive is only weakly reflected in the dcLFP (e.g., GABA-induced inhibition of action potentials).

In making the observation that under conditions of predominant layer V pyramidal neurons drive, the BOLD signal is better correlated with action potentials, we emphasize the

following points of interpretation. These data expand our understanding of the possible modes of neural-to-hemodynamic coupling that can exist in the neocortex, in that they rest on defined activity patterns imposed on the neocortex eliciting cell-type specific patterns. These data raise questions about the common assumption that subthreshold activity is the predominant correlate of the BOLD signal. Indeed, blockade of ionotropic glutamate receptors results in significant reduction in hemodynamic responses for sensory stimulation but no reduction for channelrhodopsin-driven hemodynamic responses in a similar preparation (Scott and Murphy, 2012), further supporting the findings presented here. Our findings do not, however, suggest a specific mechanism of neural-to-hemodynamic coupling. Substantial data (Cauli et al., 2004; Gordon et al., 2008; Haydon and Carmignoto, 2006; Mulligan and MacVicar, 2004; Zonta et al., 2003) suggest that pyramidal cell activity does not directly lead to local vasodilation and increased blood volume, which in turn modulates the ratio of oxygenated to deoxygenated hemoglobin (the metrics primarily indexed by the BOLD signal). Instead, the highly synchronous activity of layer V pyramidal neurons may drive either a specific sub-type of interneuron (Cauli et al., 2004) or astrocyte (Haydon and Carmignoto, 2006) that recruits smooth muscle relaxation and the consequent hemodynamic response.

Neural spiking responses to sensory stimulation have often been modeled as having independent Poisson-like statistics (Britten et al., 1993; Shadlen and Newsome, 1998; Tolhurst et al., 1983; Vogels et al., 1989). However, particularly under conditions of deployed attention, strong stimulation, or stimulus transients, highly synchronized oscillatory activity (particularly in the gamma range) can be observed (Baddeley et al., 1997; Maimon and Assad, 2009; Mainen and Sejnowski, 1995; Nase et al., 2003). In this study, we created a neural activity profile at the two ends of a possible spectrum of observed activity patterns in neocortical neurons during sensory stimulation. The spiking activity resulting from either of these activity profiles is unlikely to occur during the processing of natural sensory perception, partly due to the extreme synchrony invoked by our stimulation, but the Poisson case is arguably closer to a "natural" response. Our results for Poisson stimulation, in particular in the range of 8–56 Hz where all the electrophysiological measures show a monotonic increase, are largely consistent with previous studies using sensory stimulation (Logothetis et al., 2001).

In conclusion, our results using opto-fMRI to probe the BOLD signal amend a growing body of literature (Desai et al., 2011; Kahn et al., 2011; Lee et al., 2010; Scott and Murphy, 2012) that leverages optogenetic control to systematically examine the relation between local changes in neural activity and hemodynamic responses. We used a transgenic model, and focused on understanding the local response. We probed these responses under conditions typically employed in human imaging, blocks of sustained stimuli, and examined in detail the correlations between the BOLD signal and neurophysiological measures. Our findings are broadly consistent with components of the BOLD response being directly linked to spiking activity (Scott and Murphy, 2012) and we demonstrate sensitivity of the hemodynamic response variations in spike rate as observed in the difference between early and late responses, Poisson and periodic drive and overall spike rate. More broadly, our findings suggest that taking advantage of cell-type-specific optoengineering in vivo (Arenkiel et al., 2007; Ayling et al., 2009; Cardin et al., 2009; Han et al., 2009; Huber et al., 2008), targeting additional cell populations (Cardin et al., 2009; Sohal et al., 2009) and using cell-type specific neural silencing (Chow et al., 2010; Han and Boyden, 2007; Zhang et al., 2007), will allow the systematic causal study of the local pre- and postsynaptic cellular components that control functional hyperemia.

4. Experimental procedures

4.1. Animals

All procedures were conducted in accordance with the National Institutes of Health guidelines and with the approval of the Committee on Animal Care at MIT. Channelrhodopsin-2 transgenic mice (Arenkiel et al., 2007) were purchased from the Jackson Labs (line 18, stock 007612, strain B6.Cg-Tg (Thy1-COP4/EYFP)18Gfng/J) and subsequently crossed with C57bl/6 mice. See Table 1 for information on animals participating in recording experiments. Electrophysiological recordings and fMRI were obtained in separate animals.

4.2. Animal anesthesia and surgery

Animals were anesthetized with isoflurane mixed with oxygen for all procedures. During preparation and craniotomy surgery anesthesia was kept at a level of 2–3%. Prior to surgical procedures and placement in an animal bed for MRI or in a stereotactic frame for electrophysiology, the animal's reflexes were tested to determine that a surgical anesthesia has been reached. Immediately prior to MRI scanning and electrophysiological recording the anesthetic level was reduced to 0.5–1% expired isoflurane. For the MRI experiment, the craniotomy was restricted to a burr-hole in the skull. For the electrophysiological recordings, a craniotomy and durotomy were made to allow positioning of the optical fiber and recording electrode.

Table 1 – Animals participating in electrophysiological and fMRI experiments.

	Animals	Poisson	Periodic	Total number of runs
BOLD	4	16	16	32
SUA	6 (13)[a]	26	26	52
MUA	3[c]	8	8	16
LFP	3	18	18	36
dcLFP	3 (12)[b]	12	12	24

BOLD – blood oxygenation level-dependent; SUA—single-unit activity; MUA—multi-unit activity; LFP—local field potentials; dcLFP—direct current LFP.

[a] In parentheses the number of individual cells recorded is denoted.

[b] Number of pipette recordings is denoted in parentheses.

[c] One animal MUA data were excluded due to noise.

4.3. Light stimulation

Light stimulation was generated by a 473 nm laser (Shanghai Dream Lasers) controlled by a computer. Optical stimulation was delivered via a 200 μm diameter unjacketed optical fiber with 0.48 NA (Thorlabs) positioned at the cortical surface at a power range of 10–15 mW at the tip of the fiber, positioned over primary somatosensory cortex (SI; Bregma AP -1.5, ML 2.5).

4.4. MRI procedures

Mice were fixed to an animal bed (Bruker BioSpin MRI GmbH) using a custom tooth-piece and ear bars. Breathing rate (Small Animal Monitoring 1025, SA Instruments) and expired isoflurane (V9004 Capnograph Series) were continuously monitored. Imaging was performed on a 9.4T BioSpec 94/20 USR MRI (Bruker BioSpin MRI GmbH) that operates at a maximum gradient strength of 675 mT/m, maximum slew rate 4673 T/m/s and a rise time of 130 μs. A single transmit and receive surface coil consisting of a single copper loop and etched circuit board (20 mm diameter) was positioned over the head. To reduce susceptibility artifacts, the skin above the entire skull was removed, and the craniotomy was restricted to a small burr-hole (500 μm in diameter) and the dura was kept intact. The fiber was placed adjacent to or contacting the dura. Although care was taken to avoid it, in some animals it can be seen that the fiber is pressing on the dura compressing the superficial edge of the brain. The consistency of results across animals suggests that this has not affected the ability to drive responses locally. Functional data were acquired using a spin-echo echo-planar sequence (SE-EPI; repetition time = 2.5 s; echo time = 12.17 ms; 10 coronal slices, 200 × 200 × 500 μm). High-resolution T_1- and T_2-weighted anatomical images were recorded using a rapid acquisition process with relaxation enhancement (RARE) sequence in coronal orientations (10 coronal slices, 78 × 78 × 500 μm). Image reconstruction was carried out using ParaVision 5.0 (Bruker BioSpin MRI GmbH). Preprocessing and analysis were carried out using procedures common in conventional human fMRI experiments. These preprocessing steps included removal of the first two volumes to allow for T1-equilibration, compensation of systematic slice-dependent time shifts (SPM2, Wellcome Department of Cognitive Neurology, UCL), rigid body correction for head motion within and across runs, and smoothing with a full-width half-maximum kernel of 600 μm (FSL, FMRIB, Oxford).

As can be seen in Fig. 1, an area of signal distortion and potential dropout was observed. This artifact is a result of magnetic susceptibility artifact introduced by the craniotomy. Due to the non-linear nature of the magnetic susceptibility artifact, it is difficult to quantify the laminar extent of signal dropout just based on the SE-EPI volumes. However, two reasons lead us to infer that this artifact did not affect our measurements. First, similar responses were observed across the different animals to the 'localizer' scan independent of the presence of this artifact (see also a similar experimental setup where both optogenetic and sensory sensory stimulation was used and this artifact reduced or not present, Kahn et al., 2011). Second, high-resolution (100 × 100 × 500 μm^3) fMRI data acquired in a setup similar to that used here yielded a BOLD response in *Thy1*-ChR2 mice predominately localized over layer V, with a response profile similar to that observed here (Desai et al., 2011).

For each mouse, we conducted two intermixed experimental runs. Functional "localizer" runs consisted of 15 s on–15 s off light-evoked stimulation (8 ms pulse duration at 40 Hz). The localizer runs were used to generate functional maps (but not for calculation of hemodynamic time series averages). Functional maps were computed using a fixed effects model (SPM2, Wellcome Department of Cognitive Neurology, UCL). A region of interest (ROI) consisting of activated voxels ($P < 0.05$, corrected for multiple-comparisons using family-wise error correction) immediately adjacent to the fiber position was derived for each animal separately. The ROI derived from the localizer runs was then used to estimate the hemodynamic response for the target experimental conditions. Laser-stimulation pulse duration and frequency were 2.7 ms at 8–80 Hz. ROI analysis and statistics were carried out with in-house routines (Matlab, The Mathworks). Reported percent signal modulation is the percent difference of the BOLD signal during stimulation relative to no-stimulation periods. Reported integrated BOLD response is the area under the curve for the stated interval.

4.5. Electrophysiology

Mice were anesthetized with isoflurane and held in place with a head post cemented to the skull. A small craniotomy was made over barrel cortex (Bregma AP −1.5, ML 2.5). Whole-brain EEG was recorded by two epidural tungsten wires placed approximately 1 mm anterior of Bregma and posterior of Lambda. Stimulus control and data acquisition (except LFP and MUA recordings using Cheetah Software, Neuralynx) were performed using software custom-written in LabView (National Instruments) and Matlab (The Mathworks).

4.5.1. Cell-attached recordings

Electrodes (10–14 MΩ resistance) were pulled on a Sutter P-97 and filled with saline. Electrodes were lowered under positive pressure while injecting small amplitude current pulses. After formation of a medium resistance seal (≥80 MΩ) and verification of occurrence of spikes, the cell-attached recording configuration was achieved (MultiClamp 700B, Molecular Devices).

4.5.2. Intracellular recordings

Electrodes (5–8 MΩ resistance) were pulled on a Sutter P-97 and filled with internal patch solution (130 mM K-Gluconate, 4 mM KCl, 2 mM NaCl, 10 mM Hepes, 0.2 mM EGTA, 10 mM Phosphocreatine, 4 mM MgATP, 0.3 mM NA3GTP, adjusted to pH 7.25 with KOH and 292 mOsm with ddH_2O). Electrodes were lowered under positive pressure while injecting small amplitude current pulses until a cell was encountered and gentle suction was applied until a gigaseal was formed. Next, the cell membrane was broken and whole-cell recording configuration achieved.

4.5.3. Direct current LFP recordings

Electrodes (500–800 kΩ resistance) were pulled on a Sutter P-97 and filled with saline. Electrodes were lowered and local field potentials were recorded unfiltered in DC mode

(MultiClamp 700B, Molecular Devices). Local field potentials (LFPs) and multi-unit activity (MUA) recordings Laminar electrodes (Neuronexus Technologies) were connected to a Cheetah32 data acquisition system (Neuralynx). Electrodes consisted of 16 contacts with a diameter of 15 μm and spaced 100 μm apart. Recordings were performed under the most permissive filter settings (0.1–9000 Hz) and separated into LFP and MUA signals post-hoc.

4.5.4. *Electrophysiology analysis*

Cell-attached recording data was band-pass filtered between 600 Hz and 6000 Hz and spike times were extracted where the potential exceeded 10 standard deviations of the signal during the entire block. MUA data were extracted from laminar recordings by band-pass filtering the signal between 600 and 6000 Hz and spike times were extracted where the potential exceeded 4 standard deviations of the signal during the entire block. All firing rate data were binned at 100 ms. The dcLFP amplitudes were calculated by subtracting any slow drift in the potential (piece-wise linear fit to the potential at the beginning of each trial) and averaging the negative of the signal during the period indicated in each case, usually during the entire stimulus presentation, or in 100 ms bins for time-series analyses. For both LFP and dcLFP power, the signal was low-pass filtered at 300 Hz. Spectrograms were computed for each trial using a 250 ms Hamming window and frequencies from 7 to 200 Hz. Power spectrum density ratios were obtained by normalizing each data point by the average power of the same frequency during the 10 s pre-stimulus period. Values reported represent the average over all frequencies and the entire stimulus presentation time, or 250 ms bins for time-series analyses.

4.6. *Statistical procedures*

We tested the data for normality using the Lilliefors test (Lilliefors, 1967). Only the fMRI BOLD data exhibited non-normal distribution ($P<0.001$). Therefore, we conducted non-parametric tests throughout (Wilcoxon signed rank and rank-sum two-tail tests). Multi-way analysis of variance (ANOVA) was conducted with standard parametric ANOVA after applying a rank transform to the BOLD data (Akritas, 1990; Hollander and Wolfe, 1999). Transfer functions were computed as minimum least squared error fits between first and second order polynomials of the electrophysiological measures during early or late periods (5 stimulation frequencies $\times 2$ patterns $=10$ data points each) and the corresponding BOLD response. The time periods used in computing the transfer functions were determined from the canonical HRF. Its peak was at the 5 s time point, and the cumulative HRF from 0 to 7.5 s accounted for 96% of the total response. Thus, for the early period, the transfer function input was the first data point for each measure (corresponding to 0–100 ms for amplitudes and 0–250 ms for power ratios), and the output was the integrated BOLD response from 0 to 7.5 s. For the late period, we averaged responses during the nearly constant sustained response, i.e. 5–15 s for physiological measures and 10–20 s for BOLD.

Acknowledgments

This work was supported by the National Science Foundation, National Institutes of Health, the Howard Hughes Medical Institute, and the McGovern Institute for Brain Research.

REFERENCES

Akritas, M.G., 1990. The rank transform method in some two-factor designs. J. Am. Stat. Assoc. 85, 73–78.

Arenkiel, B.R., Peca, J., Davison, I.G., Feliciano, C., Deisseroth, K., Augustine, G.J., Ehlers, M.D., Feng, G., 2007. In vivo light-induced activation of neural circuitry in transgenic mice expressing channelrhodopsin-2. Neuron 54, 205–218.

Ayling, O.G., Harrison, T.C., Boyd, J.D., Goroshkov, A., Murphy, T.H., 2009. Automated light-based mapping of motor cortex by photoactivation of channelrhodopsin-2 transgenic mice. Nat. Methods 6, 219–224.

Baddeley, R., Abbott, L.F., Booth, M.C., Sengpiel, F., Freeman, T., Wakeman, E.A., Rolls, E.T., 1997. Responses of neurons in primary and inferior temporal visual cortices to natural scenes. Proc. Biol. Sci. 264, 1775–1783.

Boyden, E.S., Zhang, F., Bamberg, E., Nagel, G., Deisseroth, K., 2005. Millisecond-timescale, genetically targeted optical control of neural activity. Nat. Neurosci. 8, 1263–1268.

Boynton, G.M., Engel, S.A., Glover, G.H., Heeger, D.J., 1996. Linear systems analysis of functional magnetic resonance imaging in human V1. J. Neurosci. 16, 4207–4221.

Britten, K.H., Shadlen, M.N., Newsome, W.T., Movshon, J.A., 1993. Responses of neurons in macaque MT to stochastic motion signals. Vis. Neurosci. 10, 1157–1169.

Cardin, J.A., Carlen, M., Meletis, K., Knoblich, U., Zhang, F., Deisseroth, K., Tsai, L.H., Moore, C.I., 2009. Driving fast-spiking cells induces gamma rhythm and controls sensory responses. Nature 459, 663–667.

Cauli, B., Tong, X.K., Rancillac, A., Serluca, N., Lambolez, B., Rossier, J., Hamel, E., 2004. Cortical GABA interneurons in neurovascular coupling: relays for subcortical vasoactive pathways. J. Neurosci. 24, 8940–8949.

Chow, B.Y., Han, X., Dobry, A.S., Qian, X., Chuong, A.S., Li, M., Henninger, M.A., Belfort, G.M., Lin, Y., Monahan, P.E., Boyden, E.S., 2010. High-performance genetically targetable optical neural silencing by light-driven proton pumps. Nature 463, 98–102.

Connors, B.W., Gutnick, M.J., 1990. Intrinsic firing patterns of diverse neocortical neurons. Trends Neurosci. 13, 99–104.

Dale, A.M., Buckner, R.L., 1997. Selective averaging of rapidly presented individual trials using fMRI. Hum. Brain Mapp. 5, 329–340.

Desai, M., Kahn, I., Knoblich, U., Bernstein, J., Atallah, H., Yang, A., Kopell, N., Buckner, R.L., Graybiel, A.M., Moore, C.I., Boyden, E. S., 2011. Mapping brain networks in awake mice using combined optical neural control and fMRI. J. Neurophysiol. 105, 1393–1405.

Fournier, G.N., Semba, K., Rasmusson, D.D., 2004. Modality- and region-specific acetylcholine release in the rat neocortex. Neuroscience 126, 257–262.

Goense, J.B., Logothetis, N.K., 2008. Neurophysiology of the BOLD fMRI signal in awake monkeys. Curr. Biol. 18, 631–640.

Goldring, S., 1974. DC Shifts Released by Direct and Afferent Stimulation. In: Remond, A. (Ed.), Handbook of Electroencephalography and Clinical Neurophysiology, Vol.. Elsevier, pp. 12–24.

Gordon, G.R., Choi, H.B., Rungta, R.L., Ellis-Davies, G.C., MacVicar, B.A., 2008. Brain metabolism dictates the polarity of astrocyte control over arterioles. Nature 456, 745–749.

Han, X., Boyden, E.S., 2007. Multiple-color optical activation, silencing, and desynchronization of neural activity, with single-spike temporal resolution. PLoS One 2, e299.

Han, X., Qian, X., Bernstein, J.G., Zhou, H.H., Franzesi, G.T., Stern, P., Bronson, R.T., Graybiel, A.M., Desimone, R., Boyden, E.S., 2009. Millisecond-timescale optical control of neural dynamics in the nonhuman primate brain. Neuron 62, 191–198.

Haydon, P.G., Carmignoto, G., 2006. Astrocyte control of synaptic transmission and neurovascular coupling. Physiol. Rev. 86, 1009–1031.

He, B.J., Raichle, M.E., 2009. The fMRI signal, slow cortical potential and consciousness. Trends Cognitive Sci. 13, 302–309.

Heeger, D.J., Huk, A.C., Geisler, W.S., Albrecht, D.G., 2000. Spikes versus BOLD: what does neuroimaging tell us about neuronal activity?. Nat. Neurosci. 3, 631–633.

Heeger, D.J., Ress, D., 2002. What does fMRI tell us about neuronal activity?. Nat. Rev. Neurosci. 3, 142–151.

Hollander, M., Wolfe, D.A., 1999. Nonparametric statistical methods, Wiley Series in Probability and Statistics. Texts and References Section. Wiley, New York.

Huber, D., Petreanu, L., Ghitani, N., Ranade, S., Hromadka, T., Mainen, Z., Svoboda, K., 2008. Sparse optical microstimulation in barrel cortex drives learned behaviour in freely moving mice. Nature 451, 61–64.

Ishizuka, T., Kakuda, M., Araki, R., Yawo, H., 2006. Kinetic evaluation of photosensitivity in genetically engineered neurons expressing green algae light-gated channels. Neurosci. Res. 54, 85–94.

Kahn, I., Desai, M., Knoblich, U., Bernstein, J., Henninger, M., Graybiel, A.M., Boyden, E.S., Buckner, R.L., Moore, C.I., 2011. Characterization of the functional MRI response temporal linearity via optical control of neocortical pyramidal neurons. J. Neurosci. 31, 15086–15091.

Kirifides, M.L., Simpson, K.L., Lin, R.C., Waterhouse, B.D., 2001. Topographic organization and neurochemical identity of dorsal raphe neurons that project to the trigeminal somatosensory pathway in the rat. J. Comp. Neurol. 435, 325–340.

Lee, J.H., Durand, R., Gradinaru, V., Zhang, F., Goshen, I., Kim, D.S., Fenno, L.E., Ramakrishnan, C., Deisseroth, K., 2010. Global and local fMRI signals driven by neurons defined optogenetically by type and wiring. Nature 465, 788–792.

Lilliefors, H.W., 1967. On the Kolmogorov–Smirnov test for normality with mean and variance unknown. J. Am. Stat. Assoc. 62, 399–402.

Logothetis, N.K., Pauls, J., Augath, M., Trinath, T., Oeltermann, A., 2001. Neurophysiological investigation of the basis of the fMRI signal. Nature 412, 150–157.

Logothetis, N.K., 2008. What we can do and what we cannot do with fMRI. Nature 453, 869–878.

Maimon, G., Assad, J.A., 2009. Beyond Poisson: increased spike-time regularity across primate parietal cortex. Neuron 62, 426–440.

Mainen, Z.F., Sejnowski, T.J., 1995. Reliability of spike timing in neocortical neurons. Science 268, 1503–1506.

Miezin, F.M., Maccotta, L., Ollinger, J.M., Petersen, S.E., Buckner, R.L., 2000. Characterizing the hemodynamic response: effects of presentation rate, sampling procedure, and the possibility of ordering brain activity based on relative timing. Neuroimage 11, 735–759.

Moore, C.I., Nelson, S.B., Sur, M., 1999. Dynamics of neuronal processing in rat somatosensory cortex. Trends Neurosci. 22, 513–520.

Moore, C.I., 2004. Frequency-dependent processing in the vibrissa sensory system. J. Neurophysiol. 91, 2390–2399.

Mukamel, R., Gelbard, H., Arieli, A., Hasson, U., Fried, I., Malach, R., 2005. Coupling between neuronal firing, field potentials, and FMRI in human auditory cortex. Science 309, 951–954.

Mulligan, S.J., MacVicar, B.A., 2004. Calcium transients in astrocyte endfeet cause cerebrovascular constrictions. Nature 431, 195–199.

Nagel, G., Szellas, T., Huhn, W., Kateriya, S., Adeishvili, N., Berthold, P., Ollig, D., Hegemann, P., Bamberg, E., 2003. Channelrhodopsin-2, a directly light-gated cation-selective membrane channel. Proc. Natl. Acad. Sci. USA 100, 13940–13945.

Nase, G., Singer, W., Monyer, H., Engel, A.K., 2003. Features of neuronal synchrony in mouse visual cortex. J. Neurophysiol. 90, 1115–1123.

Rees, G., Friston, K., Koch, C., 2000. A direct quantitative relationship between the functional properties of human and macaque V5. Nat. Neurosci. 3, 716–723.

Schummers, J., Yu, H., Sur, M., 2008. Tuned responses of astrocytes and their influence on hemodynamic signals in the visual cortex. Science 320, 1638–1643.

Scott, N.A., Murphy, T.H., 2012. Hemodynamic responses evoked by neuronal stimulation via channelrhodopsin-2 can be independent of intracortical glutamatergic synaptic transmission. PloS One 7, e29859.

Shadlen, M.N., Newsome, W.T., 1998. The variable discharge of cortical neurons: implications for connectivity, computation, and information coding. J. Neurosci. 18, 3870–3896.

Shima, K., Nakahama, H., Yamamoto, M., 1986. Firing properties of two types of nucleus raphe dorsalis neurons during the sleep-waking cycle and their responses to sensory stimuli. Brain Res. 399, 317–326.

Shmuel, A., Augath, M., Oeltermann, A., Logothetis, N.K., 2006. Negative functional MRI response correlates with decreases in neuronal activity in monkey visual area V1. Nat. Neurosci. 9, 569–577.

Simons, D.J., Carvell, G.E., 1989. Thalamocortical response transformation in the rat vibrissa/barrel system. J. Neurophysiol. 61, 311–330.

Sirotin, Y.B., Das, A., 2009. Anticipatory haemodynamic signals in sensory cortex not predicted by local neuronal activity. Nature 457, 475–479.

Sohal, V.S., Zhang, F., Yizhar, O., Deisseroth, K., 2009. Parvalbumin neurons and gamma rhythms enhance cortical circuit performance. Nature 459, 698–702.

Swadlow, H.A., 1989. Efferent neurons and suspected interneurons in S-1 vibrissa cortex of the awake rabbit: receptive fields and axonal properties. J. Neurophysiol. 62, 288–308.

Tolhurst, D.J., Movshon, J.A., Dean, A.F., 1983. The statistical reliability of signals in single neurons in cat and monkey visual cortex. Vision Res. 23, 775–785.

Viswanathan, A., Freeman, R.D., 2007. Neurometabolic coupling in cerebral cortex reflects synaptic more than spiking activity. Nat. Neurosci. 10, 1308–1312.

Vogels, R., Spileers, W., Orban, G.A., 1989. The response variability of striate cortical neurons in the behaving monkey. Exp. Brain Res. 77, 432–436.

Wang, X., Lou, N., Xu, Q., Tian, G.F., Peng, W.G., Han, X., Kang, J., Takano, T., Nedergaard, M., 2006. Astrocytic Ca^{2+} signaling evoked by sensory stimulation in vivo. Nat. Neurosci. 9, 816–823.

Wark, B., Lundstrom, B.N., Fairhall, A., 2007. Sensory adaptation. Curr. Opin. Neurobiol. 17, 423–429.

Zhang, F., Wang, L.P., Brauner, M., Liewald, J.F., Kay, K., Watzke, N., Wood, P.G., Bamberg, E., Nagel, G., Gottschalk, A., Deisseroth, K., 2007. Multimodal fast optical interrogation of neural circuitry. Nature 446, 633–639.

Zonta, M., Angulo, M.C., Gobbo, S., Rosengarten, B., Hossmann, K. A., Pozzan, T., Carmignoto, G., 2003. Neuron-to-astrocyte signaling is central to the dynamic control of brain microcirculation. Nat. Neurosci. 6, 43–50.